Phys. Med. Biol. **45** (2000) 3489–3508. Printed in the UK PII: S0031-9155(00)12028-7

Analytic method based on identification of ellipse parameters for scanner calibration in cone-beam tomography

Frédéric Noo†‡¶, Rolf Clackdoyle‡, Catherine Mennessier§,
Timothy A White‖ and Timothy J Roney‖

† Institut d'Electricité Montefiore, Université de Liège, Belgium
‡ Department of Radiology, University of Utah, USA
§ Université J. Fourier, Grenoble, France
‖ Idaho National Engineering and Environmental Laboratory, USA

E-mail: noo@montefiore.ulg.ac.be

Received 21 February 2000, in final form 21 August 2000

Abstract. This paper is about calibration of cone-beam (CB) scanners for both x-ray computed tomography and single-photon emission computed tomography. Scanner calibration refers here to the estimation of a set of parameters which fully describe the geometry of data acquisition. Such parameters are needed for the tomographic reconstruction step. The discussion is limited to the usual case where the cone vertex and planar detector move along a circular path relative to the object. It is also assumed that the detector does not have spatial distortions. We propose a new method which requires a small set of measurements of a simple calibration object consisting of two spherical objects, that can be considered as 'point' objects. This object traces two ellipses on the detector and from the parametric description of these ellipses, the calibration geometry can be determined analytically using explicit formulae. The method is robust and easy to implement. However, it is not fully general as it is assumed that the detector is parallel to the rotation axis of the scanner. Implementation details are given for an experimental x-ray CB scanner.

1. Introduction

This paper concerns the problem of estimating a set of parameters which fully describe the geometry of a cone-beam (CB) scanner. Such parameters are needed for the tomographic image reconstruction step. We refer to this parameter estimation problem as the scanner calibration problem.

CB scanners provide data in the form of CB projections of a density function which describes the object under study. A CB projection is a set of line integrals diverging from a single point called the cone vertex (see figure 1). CB projections are generally measured for a number of positions of the cone vertex along some trajectory.

CB tomography has applications in x-ray computed tomography imaging (CT) for medical diagnostics and industrial non-destructive evaluation, and also has applications in single-photon emission computed tomography (SPECT) for medical diagnostics. In CT, the cone vertex represents the x-ray source and CB projections can be collected as radiographs, using an area detector placed so that the object is between the source and the detector. In SPECT, the cone vertex is the focal point of a collimator which could be of converging type (Gullberg *et al* 1992)

¶ Address for correspondence: Applied Mathematics, Motefiore Institute, Université de Liège, B28, B-4000 Liège, Belgium.

0031-9155/00/113489+20$30.00

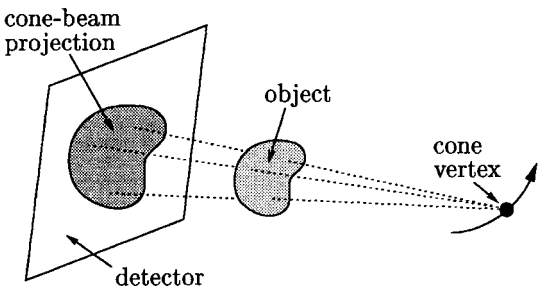

Figure 1. CB data acquisition. Line integrals of a density function describing the object are measured for all lines diverging from a single point, called the cone vertex. The result is a CB projection. Different CB projections are obtained when moving the cone vertex.

or pinhole type (Palmer and Wollmer 1990). The collimator is linked to a gamma camera that basically plays the same role as the detector in CT.

Accurate scanner calibration is important for image reconstruction. In CB tomography, it is well known that using inaccurate parameters can produce severe artefacts (see Li *et al* 1994a, b, Rizo *et al* 1994, Wang *et al* 1998). Even errors as low as 0.3° in one geometric parameter (the orientation angle of pixels in the detector plane) can have visibly detrimental effects on the reconstructed image (see White *et al* (1999) for illustrations). The purpose of this work is to describe a new method for calibration of a CB scanner. The discussion is limited to the usual case where the cone vertex and planar detector move along a circular path relative to the object. It is furthermore assumed that the area detector does not have spatial distortions. The organization of the paper is as follows. In section 2, we define the CB calibration parameters and we summarize related methods described in the literature. In section 3, we explain the principles of our calibration method, leaving the mathematical details to appendices. Section 4 concerns implementations. We illustrate results that have been obtained with real data from a CT scanner. Finally, some theoretical aspects and future perspectives are discussed with conclusions in section 5.

2. The CB calibration problem

2.1. Scanner geometry

It is convenient to consider the CB scanner as having an immobile detector and cone vertex, and that the object is placed on an imaginary turntable. The detector is assumed to be planar and to consist of regularly spaced detector elements (pixels) of known size. CB projections are collected for different angular positions of the turntable. Relative to the object, such CB projections correspond to vertex positions on a circular trajectory. Most SPECT and CT CB scanners can be viewed similarly.

To describe the geometry of the scanner, a right-handed system of Cartesian coordinates x, y and z is introduced. The z-axis is along the rotation axis of the turntable. The x-axis is along the line that contains the cone vertex and perpendicularly intersects the rotation axis. The origin of the system is at this intersection. Figure 2 illustrates the situation. In that figure, the x, y and z-directions are denoted $\underline{e}_x$, $\underline{e}_y$ and $\underline{e}_z$ respectively.

Seven parameters are sufficient to calibrate a CB scanner where the vertex motion is restricted to a circle (Rizo *et al* 1994). In this work, these seven parameters are denoted R, D, θ, ϕ, η, u_0 and v_0, and are defined as follows.

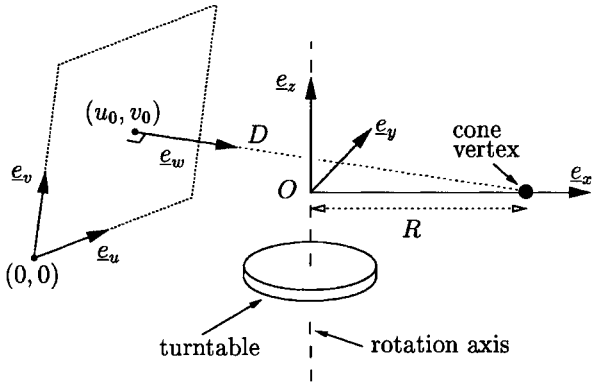

Figure 2. Scanner geometry. See detailed comments in section 2.1.

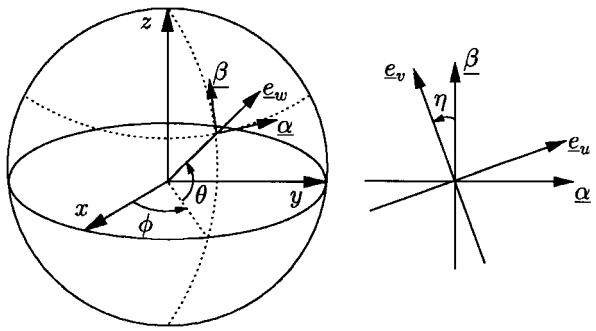

Figure 3. Orientation of detector pixels. Angles θ and ϕ specify the direction of vector $\underline{e}_w$ orthogonal to the detector plane. Vectors $\underline{\alpha}$ and $\underline{\beta}$ are perpendicular to $\underline{e}_w$; $\underline{e}_v$ is an angle η from $\underline{\beta}$.

The parameter R is the distance from the cone vertex to the rotation axis. It therefore defines the vertex position in the (x, y, z) system as $(R, 0, 0)$. Relative to the object, the vertex moves on the circle of radius R centred on the z-axis at $z = 0$, because the x-axis rotates about the z-axis.

The parameter D is the shortest distance from the vertex to the detector plane. This distance is not necessarily measured along the x-axis.

Angles $\theta \in [-\pi/2, \pi/2]$ and $\phi \in [-\pi/2, \pi/2]$ parametrize the unit vector $\underline{e}_w$ orthogonal to the detector plane. This vector specifies the direction of the shortest line segment connecting the detector to the cone vertex. Explicitly, we define

$$\underline{e}_w = (\cos\theta\cos\phi, \cos\theta\sin\phi, \sin\theta) \tag{1}$$

which states that θ and ϕ are the co-polar and azimuthal angles of $\underline{e}_w$ in the (x, y, z) space (see figures 2 and 3). For our scanner model, the condition $\theta = 0$ is assured when the turntable is horizontal while the detector plane is vertical.

Angle $\eta \in [-\pi/2, \pi/2)$ is used to define two orthogonal unit directions, $\underline{e}_u$ and $\underline{e}_v$, along which detector pixels are aligned in the detector plane. These directions are obtained by a rotation by angle η of vectors

$$\underline{\alpha} = (-\sin\phi, \cos\phi, 0) \tag{2}$$

$$\underline{\beta} = (-\sin\theta\cos\phi, -\sin\theta\sin\phi, \cos\theta) \tag{3}$$

orthogonal to $\underline{e}_w$ (see figure 3). Thus,

$$\underline{e}_u = \cos\eta\underline{\alpha} + \sin\eta\underline{\beta} \tag{4}$$

$$\underline{e}_v = \cos\eta\underline{\beta} - \sin\eta\underline{\alpha}. \tag{5}$$

Vector $\underline{\alpha}$ specifies the direction of the line of intersection of the detector and the (x, y)-plane. Note that if $\theta = 0$ (or if $\phi = 0$), then the CB projection of the rotation axis is a line on the detector parallel to $\underline{\beta}$.

Let u and v be Cartesian coordinates along vectors $\underline{e}_u$ and $\underline{e}_v$ in the detector plane. Parameters u_0 and v_0 represent the u and v distances separating the detector pixel of least u and v values ('bottom left pixel' when viewed from the cone vertex) from the orthogonal projection of the cone vertex onto the detector plane (see figure 2). For convenience, we use coordinates $(u, v) = (0, 0)$ for the bottom left detector pixel. The orthogonal projection of the cone vertex onto the detector plane is then at (u_0, v_0).

We say that the scanner is perfectly aligned when angles θ, ϕ and η are all equal to zero. With a perfectly aligned scanner, only four parameters need to be determined. We will only assume that $\theta = 0$. Our method uses measurements of a simple calibration object to estimate the six remaining geometrical parameters.

2.2. Literature overview

Methods for estimation of geometrical parameters of tomographic scanners have been investigated by many groups since 1987 (Azevedo *et al* 1999, Bronnikov 1999, Busemann-Sokole 1987, Gullberg *et al* 1987, 1990, Hsieh 1992, Li *et al* 1993, Rizo *et al* 1994, Rougée *et al* 1993, Wang *et al* 1998). Calibration aspects for the parallel-beam geometry (Azevedo *et al* 1999, Busemann-Sokole 1987) and fan-beam geometry (Gullberg *et al* 1987, Hsieh 1992) have been reported. The techniques tend to be specific to the geometry and only the overall approach of these methods has been followed for the CB case. In Gullberg *et al* (1990), Li *et al* (1993), Rizo *et al* (1994), Rougée *et al* (1993) and Wang *et al* (1998) the idea is to estimate CB geometric parameters as follows:

(a) Measure (u, v) locations where a point object (point source in SPECT, or small high-density ball in CT) placed in the field of view is projected for a number N of positions $i = 1, \ldots, N$ of the cone vertex; we denote these locations as $(\tilde{u}_i, \tilde{v}_i)$-points.

(b) Determine analytic expressions for the $(\tilde{u}, \tilde{v})$ locations found in step (a) as functions of the unknown scanner parameters and unknown positions of the point object; denoting these functions as u_i(unknowns), v_i(unknowns), this step provides a set of nonlinear equations

$$\begin{cases} \tilde{u}_i = u_i(\text{unknowns}) \\ \tilde{v}_i = v_i(\text{unknowns}) \end{cases} \qquad i = 1, \ldots, N. \tag{6}$$

(c) Solve the above equations in a least-squares sense using an iterative method, such as the Levenberg–Marquard algorithm (Press *et al* 1988).

The above approach was initially proposed for CB calibration by Gullberg *et al* (1990). In this work, it was observed that some scanner parameters are highly correlated and thus difficult to obtain from equations (6). To stabilize the inversion process, the scanner was considered to be perfectly aligned. Furthermore, it was assumed that good approximate values of the remaining four calibration parameters and point positions were available. One important result of that work was to show that R only plays the role of a magnifying factor in the reconstruction. As such, R can be *a posteriori* estimated if one knows the distance between some subobjects, such as two point objects in the reconstruction.

In Wang *et al* (1998) and Li *et al* (1993), a penalty term was incorporated in the least-squares calculation of the solution to equations (6). This penalty term was designed to hold the scanner parameters within a specified range. Good initial values for the parameters were still needed but the assumptions on the scanner geometry could be partly relaxed. Essentially, non-zero ϕ angles were permitted while η and θ were still assumed to be zero.

The method of Rizo *et al* (1994) was specific to SPECT imaging with CB collimators. They separated the scanner parameters into two classes, intrinsic parameters (D, u_0 and v_0) and extrinsic parameters (θ, ϕ and η), with R being considered separately. The intrinsic parameters describe the CB collimation, and are independent of the trajectory followed by the cone vertex. A method to establish the intrinsic parameters of a CB collimator was described. The approach involved two grids of point objects which were physically placed parallel to the collimator face. Then, using the known intrinsic collimator parameters and a single point object, the extrinsic scanner parameters could be obtained as the least-squares solution of equations (6), using coarse initial values since the extrinsic parameters are not strongly correlated. One important characteristic of the method of Rizo *et al* (1994) is that the scanner could be completely misaligned, i.e. angles θ, ϕ and η could all be non-zero.

The approach taken by Rougée *et al* (1993) was similar to that of Gullberg *et al* (1990), Li *et al* (1993) and Wang *et al* (1998), except the calibration point object was replaced by a number of point objects with known relative positions. The design of this calibration object required very high precision, but in principle better results than those in Gullberg *et al* (1990), Li *et al* (1993) and Wang *et al* (1998) could be obtained. No assumptions about angles θ, ϕ and η were made and coarse initial values could be used.

A potential weakness of all of the above methods is that they rely on a highly nonlinear parameter-estimation problem, as described by equations (6). This formulation presents the numerical difficulties of nonlinear optimization routines: the requirement for reasonable initial estimates and the possible need to carefully choose the sequence of parameters to optimize. Furthermore, there are questions of stability and uniqueness. Without further analysis, it is uncertain if local minima exist or if more than one set of calibration parameters can satisfy the equations.

In this work, we avoid these difficulties by introducing an intermediate set of parameters for which the much more straightforward estimation problem of fitting an ellipse applies. From the ellipse parameters, analytic expressions are derived for the calibration parameters. This method is robust, easy to implement, and uses a simple calibration object. However, the method is not fully general, as $\theta = 0$ is assumed.

Our method differs considerably from the direct analytic approach recently published by Bronnikov (1999). In that work the goals are different as only u_0 and ϕ are estimated, assuming angles η and θ are zero and R, D and v_0 are known. Although both methods use the same calibration object, the work described here and that of Bronnikov (1999) are complementary. Only two views are used to find u_0 and ϕ, whereas a minimum of six views are required (see below) in our method to find u_0, v_0, η, ϕ, D and R.

3. Analytic calibration

3.1. Principles

We use the scanner to collect N CB projections of a calibration object consisting of two small point objects. The number N is even and the CB projections are uniformly spaced over 360°. The two point objects must be placed well away from the rotation axis. For the most reliable performance of the algorithm, one should be at a positive z position while the other

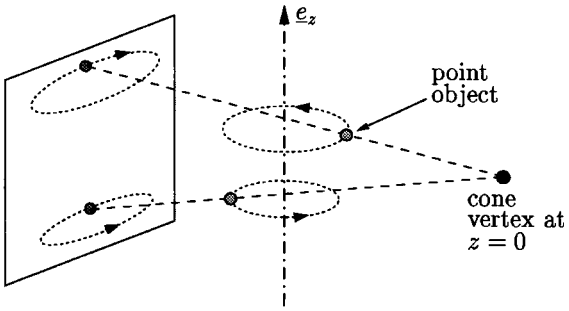

Figure 4. Calibration object. Measurements for two point objects placed in the field of view are needed to calibrate the scanner. These two points should be well away from the rotation axis and at a known distance from each other. Neither of them should be in the plane $z = 0$, where the cone vertex lies. Each point object traces an ellipse in the detector plane during data acquisition.

is at a negative z position; neither should be in or close to the plane of the cone vertex (the (x, y) plane) (see figure 4). When it is not possible to place the point objects on opposite sides of the (x, y) plane, as for example for calibration of circle scans at the top or bottom of the field-of-view (see Tam (1997) for more details on this geometry), the point objects should be placed well apart from each other in the z direction and away from the (x, y) plane. In either case (point objects on opposite or the same sides of the (x, y) plane), the distance between the two point objects must always be known accurately. This distance should be the largest possible while ensuring both point objects are in the field of view for any position of the turntable. Note that the z positions of the point objects do not need to be known.

The scanner calibration is carried out in three steps. In the first step, measurements are used to determine where the rotation axis is projected onto the detector, and the angle η is estimated using this information. Details are given in section 3.2. Once η is known, a rotation is applied to the detector pixel positions to proceed as if η were zero.

The second step consists of estimating ellipse parameters. Observe first that each point object traces a circle during data acquisition (see figure 4). Geometrically, the CB projection of the two circles yields two ellipses in the detector plane. The CB data are used to determine the equation of these ellipses. (See section 3.3 for a definition of the ellipse parameters and details on the fitting operation.)

It will be shown in section 3.4 that knowledge of the ellipse parameters and the distance separating the two point objects provides independent equations for the unknowns R, D, ϕ, u_0 and v_0. These equations can be solved analytically to obtain direct formulae for the unknowns. Straightforward application of these formulae constitutes the last calibration step.

In section 3.5, a method is provided to estimate uncertainties of the scanner parameters due to errors in the measurements.

3.2. Calculation of η

This section focuses on the determination of two particular detector locations: $(\hat{u}_1, \hat{v}_1)$ and $(\hat{u}_2, \hat{v}_2)$. These locations are defined as the CB projection of the centre of the two circles traced by the point objects during data acquisition. (Note that these locations do not generally correspond to the centre of the ellipses (see figure 5).) Geometrically, the centres of the circles lie on the rotation axis. Therefore, $(\hat{u}_1, \hat{v}_1)$ and $(\hat{u}_2, \hat{v}_2)$ are on the CB projection of the rotation axis. Also, $\hat{v}_1 \neq \hat{v}_2$ because the two point objects were placed at different z locations. When

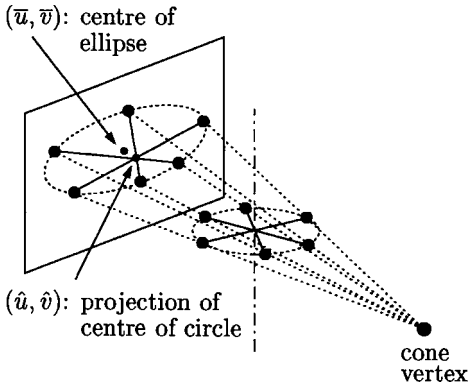

Figure 5. Definition of $(\hat{u}, \hat{v})$ and $(\overline{u}, \overline{v})$ for one point object. Point $(\hat{u}, \hat{v})$ is the projection of the centre of a circle traced by the point object in the field of view. This point lies at the intersection of all lines connecting projections of the point object for two angular positions 180° apart. Point $(\overline{u}, \overline{v})$ is the centre of the ellipse traced by the point object in the detector plane. Geometrically, $(\hat{u}, \hat{v})$ is different from $(\overline{u}, \overline{v})$.

$(\hat{u}_1, \hat{v}_1)$ and $(\hat{u}_2, \hat{v}_2)$ are known, one obtains

$$\eta = \arctan\left(\frac{\hat{u}_1 - \hat{u}_2}{\hat{v}_1 - \hat{v}_2}\right). \tag{7}$$

This equation results from two observations: the line joining $(\hat{u}_1, \hat{v}_1)$ to $(\hat{u}_2, \hat{v}_2)$ is parallel to the vector $\underline{\beta}$ because $\underline{\beta}$ is parallel to the projection of the rotation axis when $\theta = 0$, and $\underline{\beta}$ is at an angle η from $\underline{e}_v$ (see figure 3).

To obtain $(\hat{u}_1, \hat{v}_1)$ to $(\hat{u}_2, \hat{v}_2)$, we use CB measurements. Let $(u_1^{(i)}, v_1^{(i)})$ and $(u_2^{(i)}, v_2^{(i)})$, $i = 1, \ldots, N$, be the detector locations where the two point objects are projected for the N positions of the turntable. Recall that N is even and CB projections are uniformly spaced over 360°. The values of $\hat{u}_k$ and $\hat{v}_k$, with $k = 1$ or $k = 2$, are obtained as the least-squares solution of the linear equations

$$(u_k^{(j)} - u_k^{(i)})\hat{v}_k - (v_k^{(j)} - v_k^{(i)})\hat{u}_k = v_k^{(i)}u_k^{(j)} - v_k^{(j)}u_k^{(i)} \qquad j = i + N/2 \qquad i = 1, \ldots, N/2. \tag{8}$$

These equations state that all lines which connect projections of the point object k for two angular positions 180° apart (positions i and $j = i + N/2$) intersect at $(\hat{u}_k, \hat{v}_k)$ (see figure 5).

Once η is known (using (8), then (7)), a rotation is applied to the detector pixels to proceed as if η were zero. This rotation is performed about $(u, v) = (0, 0)$ and modifies u and v into

$$\begin{aligned} u^* &= u\cos\eta - v\sin\eta \\ v^* &= u\sin\eta + v\cos\eta. \end{aligned} \tag{9}$$

In particular, the unknown (u_0, v_0) becomes (u_0^*, v_0^*) and we have

$$\begin{aligned} u_0 &= u_0^*\cos\eta + v_0^*\sin\eta \\ v_0 &= -u_0^*\sin\eta + v_0^*\cos\eta. \end{aligned} \tag{10}$$

3.3. Calculation of ellipse parameters

Let $(u^{(i)}, v^{(i)}), i = 1, \ldots, N$, be the detector locations (after the transformation of equation (9)) where one point object is projected during data acquisition.

Mathematically, one can show that the $(u^{(i)}, v^{(i)})$ points lie on an ellipse. (A proof of this assertion is given in equations (26)–(30) in appendix B.) To describe the ellipse, we use the equation

$$a(u-\overline{u})^2 + b(v-\overline{v})^2 + 2c(u-\overline{u})(v-\overline{v}) = 1 \tag{11}$$

where $(\overline{u}, \overline{v})$ is the centre of the ellipse. Parameters a, b, c, $\overline{u}$ and $\overline{v}$ can be found using a linear least-squares method from estimates of the $(u^{(i)}, v^{(i)})$ points. (See appendix A for the method we use for obtaining the parameters.)

We now assume that the ellipse parameters a, b, c, $\overline{u}$, $\overline{v}$ are known for both ellipses.

3.4. Calculation of scanner parameters

In this section, equations are given which describe how the scanner parameters are calculated. The two point objects mentioned in section 3.1 are used. The ellipse parameters for the first point are a_1, b_1, c_1, $\overline{u}_1$ and $\overline{v}_1$. The parameters for the second point are a_2, b_2, c_2, $\overline{u}_2$ and $\overline{v}_2$.

In the process of calculating R, D, u_0^*, v_0^* and ϕ, some supplementary unknowns are introduced. These unknowns correspond to the radius and z-location of the circle traced during the rotation of each point object. For the first point, we use r_1 and z_1 respectively, and for the second point we use r_2 and z_2. The following equations relate the nine unknowns to the ten known ellipse parameters a_k, b_k, c_k, $\overline{u}_k$ and $\overline{v}_k$, $k = 1, 2$ (see appendix B):

$$\begin{aligned}
\overline{u}_k &= u_0^* + \frac{D\sin\phi\cos\phi}{\cos^2\phi - \rho_k^2} \\
\overline{v}_k &= v_0^* + \frac{D\zeta_k\cos\phi}{\cos^2\phi - \rho_k^2} \\
a_k &= \frac{\cos^2\phi - \rho_k^2}{\rho_k^2 D^2} \qquad b_k = \frac{a_k(1-\rho_k^2)}{\zeta_k^2} \qquad c_k = -\frac{a_k\sin\phi}{\zeta_k}
\end{aligned} \tag{12}$$

where $\rho_k = r_k/R$, and $\zeta_k = z_k/R$, $k = 1, 2$. To solve these equations for the unknowns, first note that the sign of z_k can be easily obtained by data inspection, e.g. when $z_k > 0$, one observes that the projection of the point object moves clockwise in the detector plane for a counterclockwise rotation of the turntable (see figure 4). We consider below that these sign values are known.

According to the results in appendices C and D, equations (12) can be inverted to get u_0^*, v_0^*, D, ϕ, and also ρ_k and ζ_k, $k = 1, 2$. The distance D is first calculated using the formula

$$D^2 = \frac{(a_1 - 2n_0n_1) - \varepsilon\sqrt{a_1^2 + 4n_1^2 - 4n_0n_1a_1}}{2n_1^2} \tag{13}$$

with $n_0 = (1 - m_0^2 - m_1^2)/(2m_0m_1)$ and $n_1 = (a_2 - a_1m_1^2)/(2m_0m_1)$, where

$$m_0 = (\overline{v}_2 - \overline{v}_1)\sqrt{b_2 - c_2^2/a_2} \tag{14}$$

and

$$m_1 = \sqrt{b_2 - c_2^2/a_2}/\sqrt{b_1 - c_1^2/a_1}. \tag{15}$$

In equation (13), $\varepsilon = 1$ when $z_1z_2 < 0$, that is, when the two point objects are placed on opposite sides of the plane $z = 0$. When $z_1z_2 > 0$, the situation is more complicated: one must choose between $\varepsilon = 1$ or $\varepsilon = -1$ and a physical measurement of D on the scanner may be needed to make the correct choice. Appendix D contains a short discussion of this case.

Once D is known, the other unknowns are given by the following equations:

$$\begin{aligned}
v_0^* &= \overline{v}_1 - \operatorname{sign}(z_1)\sqrt{a_1 + a_1^2 D^2}/\sqrt{a_1 b_1 - c_1^2} \\
u_0^* &= \frac{1}{2}\overline{u}_1 + \frac{1}{2}\overline{u}_2 + \frac{c_1}{2a_1}(\overline{v}_1 - v_0^*) + \frac{c_2}{2a_2}(\overline{v}_2 - v_0^*) \\
\rho_k &= \sqrt{a_k b_k - c_k^2}/\sqrt{a_k b_k + a_k^2 b_k D^2 - c_k^2} \qquad k = 1, 2 \\
\zeta_k &= D \operatorname{sign}(z_k) a_k \sqrt{a_k}/\sqrt{a_k b_k + a_k^2 b_k D^2 - c_k^2} \qquad k = 1, 2 \\
\sin\phi &= -\frac{c_1}{2a_1}\zeta_1 - \frac{c_2}{2a_2}\zeta_2.
\end{aligned} \tag{16}$$

Recall that u_0 and v_0 are obtained from u_0^* and v_0^* using (10).

The value of R, and thereby the value of r_k and z_k, $k = 1, 2$, cannot be obtained from equations (12). To estimate these values, an extra equation is needed. Recall that R only plays the role of a magnification factor in the reconstruction (Gullberg *et al* 1990). To obtain R, we use the distance d separating the two point objects. (Recall from section 3.1 that we assume this distance is known.) As shown in appendix E, d is linked to R by the relation

$$\frac{d^2}{R^2} = \frac{1}{N}\sum_{i=1}^{N}\left\{\left(\zeta_1\frac{u_1^{(i)} - u_0^*}{v_1^{(i)} - v_0^*} - \zeta_2\frac{u_2^{(i)} - u_0^*}{v_2^{(i)} - v_0^*}\right)^2 + \left(\frac{D\zeta_1}{v_1^{(i)} - v_0^*} - \frac{D\zeta_2}{v_2^{(i)} - v_0^*}\right)^2 + (\zeta_1 - \zeta_2)^2\right\} \tag{17}$$

where $(u_1^{(i)}, v_1^{(i)})$ and $(u_2^{(i)}, v_2^{(i)})$ are, as in section 3.3, the locations of the two point objects in the ith CB projection after the transformation of equation (9). From (17), we obtain R, and then $r_k = R\rho_k$ and $z_k = R\zeta_k$, for $k = 1, 2$. Due to the specific form of equation (17), one sees that any error on d would affect the estimate of R in a proportional way.

3.5. Uncertainties of the scanner parameters

The above calibration procedure is an analytic method which provides exact results when the locations $(u_1^{(i)}, v_1^{(i)})$ and $(u_2^{(i)}, v_2^{(i)})$, $i = 1, \ldots, N$, are exactly known and $N \geqslant 6$. However, in practice, only approximate values of $(u_1^{(i)}, v_1^{(i)})$ and $(u_2^{(i)}, v_2^{(i)})$ can be obtained. In this section, we provide a method to estimate uncertainties of the calibration parameters from uncertainties in the measured locations $(u_k^{(i)}, v_k^{(i)})$, $k = 1, 2$.

Observe that by chaining together the formulae of sections 3.2, 3.3 and 3.4 each estimated parameter can be written as a function of the variables $u_1^{(i)}, v_1^{(i)}, u_2^{(i)}$ and $v_2^{(i)}$, $i = 1, \ldots, N$. For example, consider the calculation of η according to formula (7). The quantities $\hat{u}_1$ and $\hat{v}_1$ (and similarly, $\hat{u}_2$ and $\hat{v}_2$) appearing in this formula are obtained from the least-squares solution of a system of linear equations (see (8)). Using matrix notation, this system could be written as

$$A\begin{pmatrix}\hat{u}_1 \\ \hat{v}_1\end{pmatrix} = b \tag{18}$$

where the vector b and the matrix A involve the quantities $u_1^{(i)}, v_1^{(i)}, u_2^{(i)}$ and $v_2^{(i)}$. The least-squares solution of (18) can be written explicitly as

$$\begin{pmatrix}\hat{u}_1 \\ \hat{v}_1\end{pmatrix} = (A^T A)^{-1} A^T b \tag{19}$$

which means that $\hat{u}_1$ and $\hat{v}_1$ can be written as (nonlinear) functions of $u_1^{(i)}, v_1^{(i)}, u_2^{(i)}$ and $v_2^{(i)}$. The same observation holds for $\hat{u}_2$ and $\hat{v}_2$, and thus also for η.

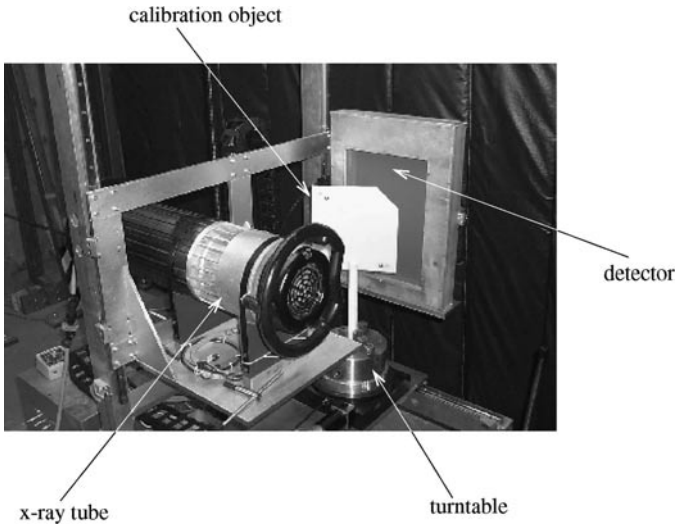

Figure 6. X-ray CB scanner currently under investigation at the Idaho National Engineering and Environmental Laboratory.

To show that the other scanner parameters (D, u_0, v_0, ϕ and R) can also be written as functions of $u_1^{(i)}$, $v_1^{(i)}$, $u_2^{(i)}$ and $v_2^{(i)}$, recall that we have analytic formulae relating D, u_0, v_0, ϕ and R to the ellipse parameters a_k, b_k, c_k, $\overline{u}_k$ and $\overline{v}_k$, where $k = 1, 2$. These ellipse parameters are obtained as explained in appendix A: first, a system of linear equations is solved in the least-squares sense to obtain intermediate quantities, called p_j, $j = 0, \ldots, 4$, from the values of $u_1^{(i)}$, $v_1^{(i)}$, $u_2^{(i)}$ and $v_2^{(i)}$; next analytic formulae are used to get a_k, b_k, c_k, $\overline{u}_k$ and $\overline{v}_k$ from these quantities. Using equations similar to (18) and (19), the quantities p_j can be written as functions of $u_1^{(i)}$, $v_1^{(i)}$, $u_2^{(i)}$ and $v_2^{(i)}$. Therefore, a_k, b_k, c_k, $\overline{u}_k$ and $\overline{v}_k$, and consequently D, u_0, v_0, ϕ and R, can in principle be written as explicit functions of $u_1^{(i)}$, $v_1^{(i)}$, $u_2^{(i)}$ and $v_2^{(i)}$.

Now, suppose that $u_1^{(i)}$, $v_1^{(i)}$, $u_2^{(i)}$ and $v_2^{(i)}$ are only known up to some common accuracy δ and let $\mathcal{A}$ be one of the parameters η, D, u_0, v_0, ϕ or R. The uncertainty $\Delta\mathcal{A}$ on $\mathcal{A}$ can be estimated using the formula

$$\Delta\mathcal{A} = \delta \sum_{i=1}^{N} \left(\left| \frac{\partial \mathcal{A}}{\partial u_1^{(i)}} \right| + \left| \frac{\partial \mathcal{A}}{\partial v_1^{(i)}} \right| + \left| \frac{\partial \mathcal{A}}{\partial u_2^{(i)}} \right| + \left| \frac{\partial \mathcal{A}}{\partial v_2^{(i)}} \right| \right) \tag{20}$$

(see, for example, Rade and Westergren (1995)).

Direct analytic calculation of the partial derivatives in (20) would be unwieldy and can be avoided because these derivatives can be reliably computed in a numerical way. For instance, to get $\partial\mathcal{A}/\partial u_1^{(1)}$ we compute the value of $\mathcal{A}$ from the quantities $u_1^{(i)}$, $v_1^{(i)}$, $u_2^{(i)}$ and $v_2^{(i)}$, using $(1+\epsilon)u_1^{(1)}$ instead of $u_1^{(1)}$, and again using $(1-\epsilon)u_1^{(1)}$ instead of $u_1^{(1)}$, where ϵ is a small number. The subtraction of the two resulting values of $\mathcal{A}$ followed by a division by 2ϵ provides a reliable estimate of $\partial\mathcal{A}/\partial u_1^{(1)}$ when ϵ is small enough.

4. Implementation

The discussion is focused on the calibration of an experimental x-ray CB scanner currently under investigation at the Idaho National Engineering and Environmental Laboratory

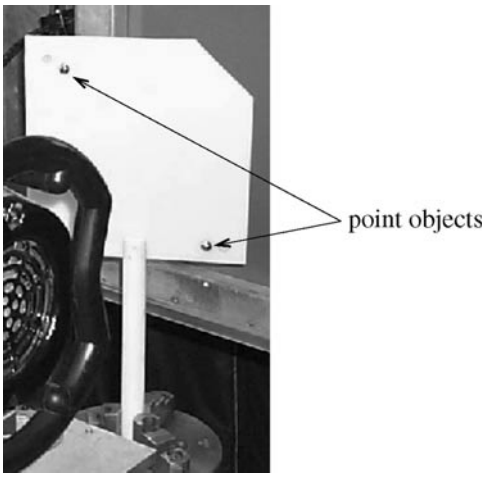

Figure 7. Calibration object. The two small high-density balls playing the role of point objects are mounted on a plastic plate.

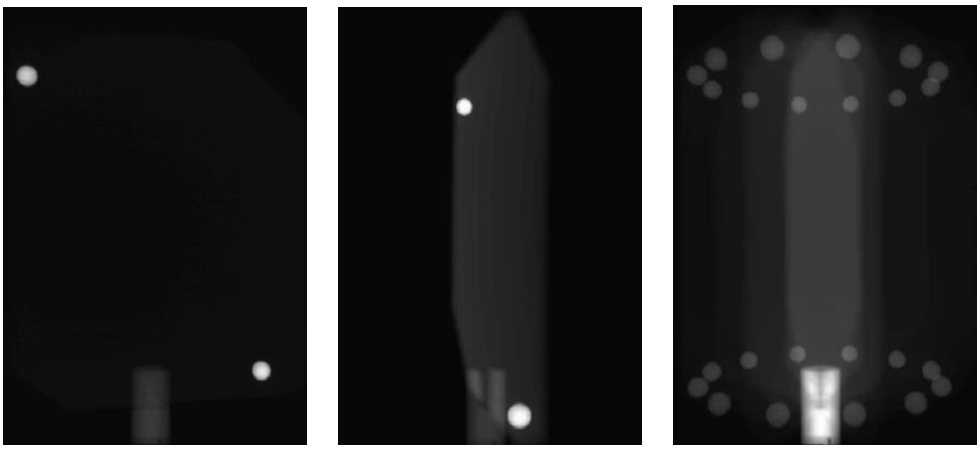

Figure 8. (Left and middle) Two typical projections of the calibration object. (Right) Superposition of 12 CB projections evenly spaced over 360°.

(see figure 6). This scanner consists of a turntable and an immobile source–detector pair, as illustrated in figure 2. The object under study is placed on the turntable and different CB projections are collected while rotating this table.

To calibrate the scanner, we first placed the turntable in the horizontal position and the detector in the vertical position, using a level, to verify the condition $\theta = 0$. Next, we collected CB projections of the calibration object shown in figure 7. Figure 8 shows two typical projections. The x-ray generator used for data collection was an industrial unit manufactured by Andrex (300 kVp/3.0 mA maximum output, fixed anode, 100% duty cycle) operated at 162 kVp and 0.5 mA. The beam was filtered with 4 mm of Al and 4.8 mm of Cu to harden it and avoid saturating the detector. The detector was a distortion-free amorphous silicon flat-panel imager (FlashScan-30 from dpiX) discretized to 2304 $\times$ 3200 pixels on a 127 μm pitch. Each pixel was digitized to 12 bits and non-uniformities in the beam profile and detector

Table 1. Ellipse parameters for $N = 6, 12, 120$ projections.

N	Ellipse (k)	a_k (mm^{-2})	b_k (mm^{-2})	c_k (mm^{-2})	$\overline{u}_k$ (mm)	$\overline{v}_k$ (mm)
12	1	8.096×10^{-5}	1.335×10^{-3}	8.986×10^{-6}	135.77	340.33
6	1	8.090×10^{-5}	1.335×10^{-3}	9.291×10^{-6}	135.67	340.35
120	1	8.093×10^{-5}	1.337×10^{-3}	9.009×10^{-6}	135.76	340.31
12	2	7.975×10^{-5}	1.199×10^{-3}	-9.291×10^{-6}	135.80	55.57
6	2	7.975×10^{-5}	1.199×10^{-3}	-9.418×10^{-6}	135.75	55.59
120	2	7.973×10^{-5}	1.199×10^{-3}	-9.227×10^{-6}	135.81	55.58

Table 2. Calibration results for different numbers N of projections.

N	η (deg)	D (mm)	u_0 (mm)	v_0 (mm)	ϕ (deg)	R (mm)	r_1 (mm)	z_1 (mm)	r_2 (mm)	z_2 (mm)
12	−0.304	553.49	150.92	202.08	−1.611	377.88	74.37	91.22	74.90	−95.52
6	−0.299	553.56	151.25	202.08	−1.650	377.90	74.39	91.21	74.90	−95.51
120	−0.305	553.82	150.88	202.10	−1.607	378.09	74.38	91.20	74.91	−95.52

readout electronics were corrected in a nonlinear image-correction algorithm. Four-by-four regions of adjacent pixels were averaged before logarithmic correction of the projections to give an effective pixel dimension of 0.508 mm. The integration time per projection was 3.4 s; this long integration time is acceptable for industrial CT applications and will decrease as detector electronics become faster. (For medical applications, a detector with a faster readout should be used along with a lower-energy x-ray beam.)

The calibration object consisted of two small stainless steel balls mounted on a plastic plate; the diameter of the balls was about 8 mm and the plastic plate was chosen as a low-density material so that the balls could be clearly distinguished in the projections for most positions of the turntable. The point objects used in the calibration method were considered to be the centres of these two stainless steel balls. For each projection i, we calculated the centroids of the images of these two balls in the detector plane to estimate the locations $(u_1^{(i)}, v_1^{(i)})$ and $(u_2^{(i)}, v_2^{(i)})$ where these point objects appeared. Next, we applied the formulae of section 3. The results are presented in tables 1 and 2. These results were successively obtained with 12, 6 and then 120 CB projections evenly spaced over 360°. We also show in figure 8 the sum of the 12 projections. This figure illustrates the motion of the two balls on ellipses during data acquisition.

Table 2 also illustrates the numerical stability of our calibration method because only very small differences were observed in the estimation of scanner parameters using different numbers of projections. In particular, for r_k and z_k, $k = 1, 2$, we note that the differences were much smaller than the detector pixel size (less than one-twentieth of the pixel size). Tables 1 and 2 also show that with accurate estimates of the ellipses, the method can perform well with only six projections. Six is the minimum number of projections required to perform calibration with our method.

As explained in section 3.5, the uncertainty of the scanner parameters depends on the accuracy to which the centroid values $u_1^{(i)}$, $v_1^{(i)}$, $u_2^{(i)}$ and $v_2^{(i)}$ can be estimated. Using formula (20) with an error of one-tenth of a pixel on these values, we obtained the uncertainties shown in table 3.

To get satisfactory results, the computation of the locations $(u_1^{(i)}, v_1^{(i)})$ and $(u_2^{(i)}, v_2^{(i)})$ must be carried out carefully, as explained below.

Table 3. Uncertainties of the scanner parameters for $N = 6, 12, 120$.

N	$\Delta\eta$ (deg)	ΔD (mm)	Δu_0 (mm)	Δv_0 (mm)	$\Delta\phi$ (deg)	ΔR (mm)	Δr_1 (mm)	Δz_1 (mm)	Δr_2 (mm)	Δz_2 (mm)
12	0.077	2.012	2.228	0.497	0.223	1.093	0.130	0.330	0.128	0.329
6	0.077	1.936	2.201	0.472	0.221	1.074	0.117	0.312	0.121	0.317
120	0.083	2.065	2.133	0.511	0.211	1.163	0.126	0.349	0.123	0.348

First, attention must be paid to the design of the calibration balls. We selected a material that is not too absorbing at the x-ray energy used to avoid getting projections which would be flat in their central part because of beam hardening. Otherwise, errors would have occurred in the centroid calculation. The size of the ball was also important: to minimize discretization errors in the centroid calculation, the balls should be projected on a large number of pixels. In our implementation, more than 400 pixels were involved in the calculation of a given centroid.

Next, care must be taken with the holding support, if any (the plastic plate, here). In this implementation, we applied a threshold to the x-ray images (projections) to remove the background intensity due to the plastic plate. The threshold was given as the smallest possible value for each projection; different projections were thus applied with different thresholds. Projections for which the threshold was higher than 20% of the maximum intensity value were disregarded.

5. Discussion and conclusions

In this work, we have proposed a new method for calibration of CB scanners that use a circular path for the cone vertex. This method is robust, easy to implement and uses a simple calibration object. It is not fully general as $\theta = 0$ is assumed, which means that the detector should be parallel to the rotation axis of the scanner. Also, any spatial distortions of the area detector should be corrected prior to using the method.

The preferred method involves positioning the calibration object so that one point projects above the plane of the cone vertex path, and the other point projects below. However, if both points must be placed on the same side of this plane, the method can still be applied, but with a few more steps to find the parameter D (see appendix D for the details).

In practice, condition $\theta = 0$ is known to be a weak requirement (Gullberg *et al* 1990, Li *et al* 1993, Wang *et al* 1998), especially because the scanner can often be aligned to meet this condition. Our future investigations will be focused on direct calculation of θ along with the other scanner parameters to permit more flexibility in data acquisition. At this stage of our research, we have observed that more than two point objects are needed to calibrate the scanner when θ is non-zero.

Errors on the estimation of the scanner parameters depend on the accuracy of the locations of the projected point objects. The precautions we took in the calculation of these locations seem to be satisfactory for calibration of CT systems. For calibration of SPECT systems, a better approach involving photon statistics might be needed for the centroid calculation (see e.g. Hsieh 1992). Uncertainties in the estimated scanner parameters can be obtained as explained in section 3.5. To test the reliability of the parameters, we also carry out successive evaluations using different sets of projections, as shown in table 2, and perform resolution tests on the reconstructions of point and rods objects, as illustrated in White *et al* (1999).

We are also exploring calibration of scanners in spiral CT and helical CB tomography. Preliminary results for a helical CB scanner are presented in Noo *et al* (2000).

Acknowledgments

FN is *chargé de recherches* with the National Fund for Scientific Research (FNRS, Belgium). This work was supported in part by the US Department of Energy, Assistant Secretary for Environmental Management, Environmental Systems Research Program, under DOE Operations Office Contract DE-AC07-94ID13223.

Appendix A

In this appendix, we explain how parameters $a, b, c, \overline{u}$ and $\overline{v}$ describing the ellipse equation (11) can be calculated when points $(u^{(i)}, v^{(i)})$, $i = 1, \ldots, N$ belonging to the ellipse are known. There are many possible methods to fit the ellipse; the one we describe here is taken from Niewenglowski (1911).

Our method involves intermediate variables p_j, $j = 0, \ldots, 4$ that allow us to rewrite the ellipse equation (11) in the form

$$p_0 u^2 + v^2 - 2p_1 u - 2p_2 v + 2p_3 uv + p_4 = 0. \tag{21}$$

These variables are related to $a, b, c, \overline{u}$ and $\overline{v}$ by the equations

$$p_0 = \frac{a}{b} \qquad p_1 = \frac{a}{b}\overline{u} + \frac{c}{b}\overline{v} \qquad p_2 = \overline{v} + \frac{c}{b}\overline{u} \qquad p_3 = \frac{c}{b}$$
$$p_4 = \frac{a}{b}\overline{u}^2 + \overline{v}^2 + 2\frac{c}{b}\overline{uv} - \frac{1}{b}. \tag{22}$$

The estimation of a, b, c, $\overline{u}$ and $\overline{v}$ is carried out in two steps. The p_j, $j = 0, \ldots, 4$ variables are first calculated as the least-squares solution of linear equations

$$p_0 (u^{(i)})^2 - 2p_1 u^{(i)} - 2p_2 v^{(i)} + 2p_3 u^{(i)} v^{(i)} + p_4 = -(v^{(i)})^2 \qquad i = 1, \ldots, N. \tag{23}$$

Next, relations (22) are inverted to get

$$\overline{u} = (p_1 - p_2 p_3)/(p_0 - p_3^2) \qquad \overline{v} = (p_0 p_2 - p_1 p_3)/(p_0 - p_3^2) \tag{24}$$

and also

$$a = p_0/(p_0\overline{u}^2 + \overline{v}^2 + 2p_3\overline{uv} - p_4) \qquad b = a/p_0 \qquad \text{and} \qquad c = p_3 b. \tag{25}$$

Note that the least-squares solution of (23) is unique only if $N \geqslant 5$. Generally, choosing $N = 5$ is sufficient to calculate the ellipse parameters. However, if $(u^{(i)}, v^{(i)})$-locations are only known up to some accuracy, as is the case in practice, better results would be obtained with increasing N values.

Appendix B

Here, we derive equations (12) that relate the geometrical parameters of the scanner to the parameters of the ellipse generated by the CB projection of a single point object rotating about the z-axis. For this discussion, it is assumed that $\eta = 0$.

We consider that the point object is initially at the location $\underline{x}_0 = (r\cos\psi_0, r\sin\psi_0, z)$ in the (x, y, z) coordinate system of figure 2. After a rotation of angle ψ about the z-axis, its position is thus $\underline{x} = (r\cos(\psi + \psi_0), r\sin(\psi + \psi_0), z)$.

For angular position ψ, the CB projection of the point source is at the (u, v) location defined by the vector equation

$$\underline{x} - R\underline{e}_x = t((u - u_0)\underline{e}_u + (v - v_0)\underline{e}_v - D\underline{e}_w). \tag{26}$$

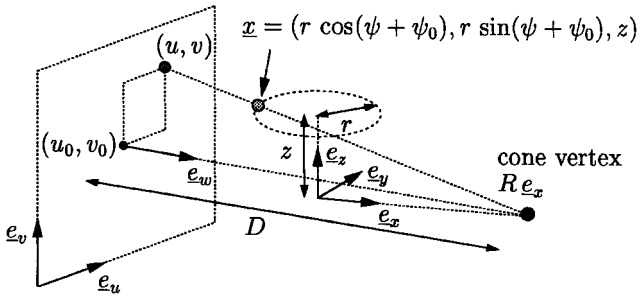

Figure 9. CB projection of a point object for a given position ψ of the turntable. At $\psi = 0$, the point object was at $\underline{x} = (r\cos\psi_0, r\sin\psi_0, z)$.

Equation (26) states that the vector from the cone vertex to the point $\underline{x}$ is a multiple, t, of the vector from the cone vertex to the CB projection of $\underline{x}$ onto the detector (see figure 9). With the definition of vectors $\underline{e}_u$, $\underline{e}_v$ and $\underline{e}_w$ given in section 2, and using $\theta = 0$ and $\eta = 0$, equation (26) leads to the following relations

$$r\cos(\psi+\psi_0) = R - t((u-u_0)\sin\phi + D\cos\phi) \tag{27}$$

$$r\sin(\psi+\psi_0) = t((u-u_0)\cos\phi - D\sin\phi) \tag{28}$$

$$z = t(v - v_0). \tag{29}$$

Note that $v \neq v_0$ since the point object does not lie in the (x, y) plane. Therefore equation (29) can be used to eliminate t in equations (27) and (28), which can be squared and summed to eliminate $\psi + \psi_0$ and obtain the ellipse equation

$$p_0U^2 + V^2 - 2p_1U - 2p_2V + 2p_3UV + p_4 = 0 \tag{30}$$

where $U = u - u_0$ and $V = v - v_0$. The variables p_j, $j = 0, \ldots, 4$ in (30) are defined as follows

$$p_0 = \frac{\zeta^2}{1-\rho^2} \qquad p_1 = 0 \qquad p_2 = \frac{\zeta D\cos\phi}{1-\rho^2} \qquad p_3 = -\frac{\zeta\sin\phi}{1-\rho^2} \qquad p_4 = \frac{\zeta^2D^2}{1-\rho^2} \tag{31}$$

with $\rho = r/R$ and $\zeta = z/R$. Using the results of appendix A, (30) can be rewritten in the form

$$a(u-\overline{u})^2 + b(v-\overline{v})^2 + 2c(u-\overline{u})(v-\overline{v}) = 1 \tag{32}$$

with

$$\overline{u} = u_0 + (p_1 - p_2p_3)/(p_0 - p_3^2) \qquad \overline{v} = v_0 + (p_0p_2 - p_1p_3)/(p_0 - p_3^2)$$
$$a = p_0/\{p_0(\overline{u}-u_0)^2 + (\overline{v}-v_0)^2 + 2p_3(\overline{u}-u_0)(\overline{v}-v_0) - p_4\} \tag{33}$$

and $b = a/p_0$, $c = p_3b$. From (31), one then obtains

$$\overline{u} = u_0 + \frac{D\sin\phi\cos\phi}{\cos^2\phi - \rho^2} \qquad \overline{v} = v_0 + \frac{D\zeta\cos\phi}{\cos^2\phi - \rho^2}$$
$$a = \frac{\cos^2\phi - \rho^2}{\rho^2D^2} \qquad b = \frac{a(1-\rho^2)}{\zeta^2} \qquad c = -\frac{a\sin\phi}{\zeta}. \tag{34}$$

These relations are those of section 3.4.

Appendix C

This appendix describes how the scanner parameters can be calculated from the nonlinear equations (12) which relate these parameters to the ellipse parameters for two point objects. Equations (12) can be rewritten as follows:

$$\overline{u}_1 = u_0 + \frac{D\sin\phi\cos\phi}{\cos^2\phi - \rho_1^2} \tag{35a}$$

$$\overline{u}_2 = u_0 + \frac{D\sin\phi\cos\phi}{\cos^2\phi - \rho_2^2} \tag{35b}$$

$$\overline{v}_1 = v_0 + \frac{D\zeta_1\cos\phi}{\cos^2\phi - \rho_1^2} \tag{35c}$$

$$\overline{v}_2 = v_0 + \frac{D\zeta_2\cos\phi}{\cos^2\phi - \rho_2^2} \tag{35d}$$

$$a_1 = \frac{\cos^2\phi - \rho_1^2}{\rho_1^2 D^2} \tag{35e}$$

$$a_2 = \frac{\cos^2\phi - \rho^2}{\rho^2 D^2} \tag{35f}$$

$$b_1 = \frac{1-\rho_1^2}{\zeta_1^2} a_1 \tag{35g}$$

$$b_2 = \frac{1-\rho_2^2}{\zeta_2^2} a_2 \tag{35h}$$

$$c_1 = \frac{-\sin\phi}{\zeta_1} a_1 \tag{35i}$$

$$c_2 = \frac{-\sin\phi}{\zeta_2} a_2. \tag{35j}$$

The unknowns are D, u_0, v_0, ϕ, ρ_1, ζ_1, ρ_2 and ζ_2.

Before solving the above equations, we recall from section 3.3 that the sign of parameters ζ_1 and ζ_2 can be easily found by inspection of the CB projections of the two point objects. We consider that these values are known.

In a first step towards inversion of equations (35), we use (35*e*), (35*g*) and (35*i*) to get ρ_1 and ζ_1 as functions of D. Noting first that $a_1 b_1 - c_1^2 = a_1^3 D^2 \rho_1^2 / \zeta_1^2 \geqslant 0$, straightforward calculations lead us to the following relations

$$\begin{aligned} \rho_1 &= \sqrt{a_1 b_1 - c_1^2} \Big/ \sqrt{a_1 b_1 + a_1^2 b_1 D^2 - c_1^2} \\ \zeta_1 &= D\,\mathrm{sign}(\zeta_1) a_1 \sqrt{a_1} \Big/ \sqrt{a_1 b_1 + a_1^2 b_1 D^2 - c_1^2}. \end{aligned} \tag{36}$$

We solve for v_0 as a function of D by starting with equation (35*c*), eliminating ϕ using (35*e*), then applying equations (36) as follows:

$$\begin{aligned} v_0 = \overline{v}_1 - \frac{D\zeta_1\cos\phi}{\cos^2\phi - \rho_1^2} &= \overline{v}_1 - \frac{D\zeta_1\rho_1\sqrt{1+a_1D^2}}{\rho_1^2 a_1 D^2} \\ &= \overline{v}_1 - \mathrm{sign}(\zeta_1)\sqrt{a_1 + a_1^2 D^2} \Big/ \sqrt{a_1 b_1 - c_1^2}. \end{aligned} \tag{37}$$

A similar sequence can be applied to find v_0 in terms of the second ellipse parameters. Equating these expressions for v_0 yields an equation in D only:

$$\overline{v}_1 - \mathrm{sign}(\zeta_1)\sqrt{a_1 + a_1^2 D^2} \Big/ \sqrt{a_1 b_1 - c_1^2} = \overline{v}_2 - \mathrm{sign}(\zeta_2)\sqrt{a_2 + a_2^2 D^2} \Big/ \sqrt{a_2 b_2 - c_2^2}. \tag{38}$$

This equation can be solved analytically as explained in appendix D. Note that another equation for D can be obtained by equating the two values of u_0 available from equations (35a) and (35b). This approach was disregarded because the resulting equation for D degenerates as ϕ tends to zero.

Once D is known from (38), all the other parameters can be calculated as follows. We first get

$$v_0 = v_1 - \text{sign}(\zeta_1)\sqrt{a_1 + a_1^2 D^2}/\sqrt{a_1 b_1 - c_1^2}. \tag{39}$$

Next, we use (36) to get ρ_1, ζ_1, and analogously for ρ_2 and ζ_2. Angle ϕ can be either obtained from (35i) or (35j), i.e.

$$\sin\phi = -\frac{c_1}{a_1}\zeta_1 \qquad \text{or} \qquad \sin\phi = -\frac{c_2}{a_2}\zeta_2. \tag{40}$$

This situation shows the existence of a certain redundancy of information in equations (35). We use this redundancy to improve accuracy of the ϕ value by averaging available estimates, i.e. we take

$$\sin\phi = -\frac{c_1}{2a_1}\zeta_1 - \frac{c_2}{2a_2}\zeta_2. \tag{41}$$

Parameter u_0 can also be obtained in two different ways. Using (35a), (35c) and (35i), we get

$$u_0 = \overline{u}_1 - \frac{D\sin\phi\cos\phi}{\cos^2\phi - \rho_1^2} = \overline{u}_1 + \frac{c_1}{a_1}(\overline{v}_1 - v_0). \tag{42}$$

Or else, using (35b), (35d) and (35j), we get

$$u_0 = \overline{u}_2 - \frac{D\sin\phi\cos\phi}{\cos^2\phi - \rho_2^2} = \overline{u}_2 + \frac{c_2}{a_2}(\overline{v}_2 - v_0). \tag{43}$$

In the presence of errors in the ellipse parameters, (42) and (43) will produce slightly different estimates for u_0. To improve accuracy on u_0, we average available estimates, i.e. we calculate:

$$u_0 = \frac{1}{2}\overline{u}_1 + \frac{1}{2}\overline{u}_2 + \frac{c_1}{2a_1}(\overline{v}_1 - v_0) + \frac{c_2}{2a_2}(\overline{v}_2 - v_0). \tag{44}$$

Appendix D

This appendix provides mathematical details of the calculation of D from equation (38). Observe first that this equation is quadratic in $x = D^2$ and admits thus at most two solutions. To solve (38), we introduce intermediate quantities

$$m_0 = (\overline{v}_2 - \overline{v}_1)\sqrt{b_2 - c_2^2/a_2} \tag{45}$$

and

$$m_1 = \sqrt{b_2 - c_2^2/a_2}/\sqrt{b_1 - c_1^2/a_1}. \tag{46}$$

Using these definitions, equation (38) can be written in the form

$$\sqrt{1 + a_2 x} = \text{sign}(z_2)(m_0 + m_1\,\text{sign}(z_1)\sqrt{1 + a_1 x}). \tag{47}$$

Squaring both sides of this equation, we get

$$\sqrt{1 + a_1 x} = \text{sign}(z_1)(n_0 + n_1 x) \tag{48}$$

with $n_0 = (1 - m_0^2 - m_1^2)/(2m_0 m_1)$ and $n_1 = (a_2 - a_1 m_1^2)/(2m_0 m_1)$. Squaring again both sides of (48), we obtain the equation

$$n_1^2 x^2 + (2n_0 n_1 - a_1)x + n_0^2 - 1 = 0. \tag{49}$$

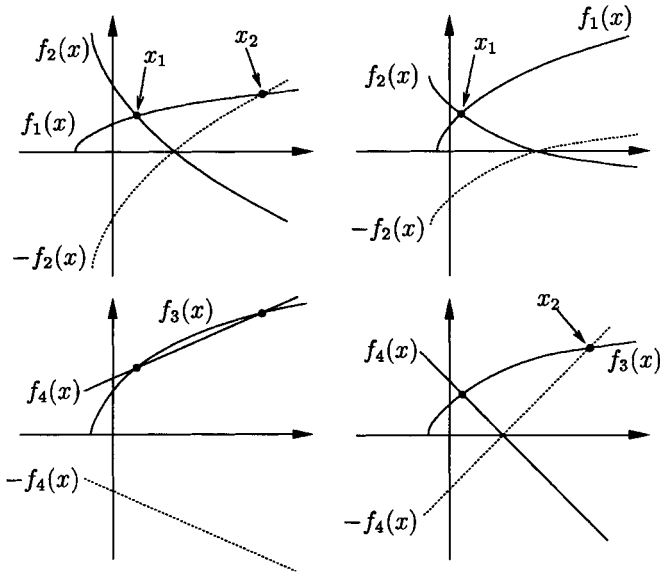

Figure 10. Graphical construction of x_1 and x_2 when $m_1 < 0$. On the left: x_2 appears when squaring both sides of (47). On the right: x_2 appears when squaring both sides of (48). In each case, the correct root is x_1.

The solutions of this equation are

$$x_1 = \frac{a_1 - 2n_0n_1 - \sqrt{\Delta}}{2n_1^2} \qquad \text{and} \qquad x_2 = \frac{a_1 - 2n_0n_1 + \sqrt{\Delta}}{2n_1^2} \tag{50}$$

with $\Delta = a_1^2 + 4n_1^2 - 4n_0n_1a_1$. To be solutions of (47), x_1 and x_2 must satisfy the conditions

$$\text{sign}(z_1)(n_0 + n_1x) > 0 \qquad \text{and} \qquad \text{sign}(z_2)(m_0 + m_1\,\text{sign}(z_1)\sqrt{1 + a_1x}) > 0. \tag{51}$$

Note that $x_1 < x_2$.

Geometrically, the solutions of (47) are at the intersections of two half-parabolas. When z_1 and z_2 have opposite signs, these half-parabolas have opposite convexities (m_1 is a positive number). Therefore, (47) admits at most one solution. For physical reasons, there must be one positive solution; this solution is x_1 and thus $D = \sqrt{x_1}$. The situation is illustrated in figure 10. In this figure, $f_1(x) = \sqrt{1 + a_2x}$, $f_2(x) = \text{sign}(z_2)(m_0 + m_1\,\text{sign}(z_1)\sqrt{1 + a_1x})$, $f_3(x) = \sqrt{1 + a_1x}$ and $f_4(x) = \text{sign}(z_1)(n_0 + n_1x)$. To draw the graphs of $f_1(x)$, $f_2(x)$, $f_3(x)$ and $f_4(x)$, note that with $z_1z_2 < 0$, the condition $f_2(0) > f_1(0)$ (i.e. $\text{sign}(z_2)(m_0 + m_1\,\text{sign}(z_1)) > 1$) is required to guarantee that equation (47) admits a positive root. Also, from the definition of n_0, $\text{sign}(z_2)(m_0 + m_1\,\text{sign}(z_1)) > 1$ implies $\text{sign}(z_1)n_0 > 1$, i.e. $f_4(0) > f_3(0)$. Mathematically, the spurious root can be introduced either when squaring both sides of (47) or when squaring both sides of (48). In both cases, as shown in figure 10, this spurious root will be the largest root of (49), i.e. x_2.

When z_1 and z_2 have the same sign, the situation is more complicated and no simple rule was found to choose between x_1 and x_2. Conditions (51) have to be checked. Usually, (51) will identify a spurious solution, and D can be uniquely found. However, it is also possible for x_1 and x_2 to both satisfy (47), and two values are then available for D. This situation is only likely to arise in unusual circumstances, such as both point objects being placed at close z and r locations. When this occurs, a physical measurement of D on the scanner may be needed to identify the correct value.

Appendix E

In this appendix, we derive equation (17) that relates the parameter R to the distance d between the two point objects. We consider that these two objects are initially at

$$\underline{x}_k = (r_k \cos\omega_k, r_k \sin\omega_k, z_k) \qquad k = 1, 2. \tag{52}$$

After a rotation of angle ψ about the z-axis, their positions are thus

$$\underline{x}_k = (r_k \cos(\omega_k + \psi), r_k \sin(\omega_k + \psi), z_k) \qquad k = 1, 2. \tag{53}$$

By definition, we have

$$d^2 = (r_1 \cos(\omega_1 + \psi) - r_2 \cos(\omega_2 + \psi))^2 + (r_1 \sin(\omega_1 + \psi) - r_2 \sin(\omega_2 + \psi))^2 + (z_1 - z_2)^2. \tag{54}$$

Let $(u_k^{(i)}, v_k^{(i)})$, $k = 1, 2$ be the detector positions where the point objects are projected for some angular positions ψ_i, $i = 1, \ldots, N$. Assuming $\eta = 0$ and following the same developments as in appendix B, we can derive the relations

$$r_k \cos(\omega_k + \psi_i) = R - \frac{z_k}{v_k^{(i)} - v_0}((u_k^{(i)} - u_0)\sin\phi + D\cos\phi) \tag{55}$$

$$r_k \sin(\omega_k + \psi_i) = \frac{z_k}{v_k^{(i)} - v_0}((u_k^{(i)} - u_0)\cos\phi - D\sin\phi). \tag{56}$$

Inserting (55) and (56) into (54), direct calculations lead to the equation

$$d^2 = \left(z_1 \frac{u_1^{(i)} - u_0}{v_1^{(i)} - v_0} - z_2 \frac{u_2^{(i)} - u_0}{v_2^{(i)} - v_0}\right)^2 + \left(\frac{Dz_1}{v_1^{(i)} - v_0} - \frac{Dz_2}{v_2^{(i)} - v_0}\right)^2 + (z_1 - z_2)^2. \tag{57}$$

Or also,

$$\frac{d^2}{R^2} = \left(\zeta_1 \frac{u_1^{(i)} - u_0}{v_1^{(i)} - v_0} - \zeta_2 \frac{u_2^{(i)} - u_0}{v_2^{(i)} - v_0}\right)^2 + \left(\frac{D\zeta_1}{v_1^{(i)} - v_0} - \frac{D\zeta_2}{v_2^{(i)} - v_0}\right)^2 + (\zeta_1 - \zeta_2)^2 \tag{58}$$

with $\zeta_1 = z_1/R$ and $\zeta_2 = z_2/R$.

Equation (58) holds for all values of index i. However, when positions $(u_k^{(i)}, v_k^{(i)})$ are only known up to some accuracy, slightly different values of d^2/R^2 will be obtained for different i indices. To improve accuracy on calculation of d^2/R^2, and thereby on calculation of R, an average of all available estimates of d^2/R^2 is taken, which leads to equation (17).

References

Azevedo S G, Schnebeck D J, Fitch J P and Martz H E 1990 Calculation of the rotational centers in computed tomography sinograms *IEEE Trans. Nucl. Sci.* **37** 1525–40

Bronnikov A V 1999 Virtual alignment of x-ray cone-beam tomography system using two calibration aperture measurements *Opt. Eng.* **38** 381–6

Busemann-Sokole E 1987 Measurement of collimator hole angulation and camera head tilt for slant and parallel-hole collimators used in SPECT *J. Nucl. Med.* **28** 1592–8

Gullberg G T, Tsui B M W, Crawford C R, Ballard J G and Hagius J T 1990 Estimation of geometrical parameters and collimator evaluation for cone-beam tomography *Med. Phys.* **17** 264–72

Gullberg G T, Tsui B M W, Crawford C R and Edgerton E 1987 Estimation of geometrical parameters for fan-beam tomography *Phys. Med. Biol.* **32** 1581–94

Gullberg G T, Zeng G L, Datz F L, Christian P E, Tung C-H and Morgan H T 1992 Review of convergent beam tomography in single photon emission computed tomography *Phys. Med. Biol.* **37** 507–34

Hsieh Y-L 1992 Calibration of fan-beam geometry for single photon emission computed tomography *PhD Thesis* Department of Mechanical Engineering, University of Utah

Li J, Jaszczak R J, Greer K L and Coleman R E 1994a A filtered backprojection algorithm for pinhole SPECT with a displaced center of rotation *Phys. Med. Biol.* **39** 165–76

Li J, Jaszczak R J, Wang H, Greer K L and Coleman R E 1993 Determination of both mechanical and electronic shifts in cone-beam SPECT *Phys. Med. Biol.* **38** 743–54

Li J, Jaszczak R J, Wang H, Gullberg G T, Greer K L and Coleman R E 1994b A cone-beam SPECT reconstruction algorithm with a displaced center of rotation *Med. Phys.* **21** 145–52

Niewenglowski B 1911 *Cours de Géométrie Analytique. Tome II. Chap. XV: Détermination d'une Conique* (Paris: Gauthier-Villars) pp 260–89

Noo F, Schaller S, Clackdoyle R, White T A and Roney T J 2000 Image reconstruction from misaligned truncated helical cone-beam data *Proc. 1999 IEEE Nuclear Science Symp. and Medical Imaging Conf. (Seattle)* pp 1028–32

Palmer J and Wollmer P 1990 Pinhole emission computed tomography: method and experimental evaluation *Phys. Med. Biol.* **35** 339–50

Press W H, Flannery B P, Teukolsky S A and Vetterling W T 1988 *Numerical Recipes in C: The Art of Scientific Computing* (Cambridge: Cambridge University Press)

Rade L and Westergren B 1995 *Mathematics Handbook for Science and Engineering* (Cambridge, MA: Birkhauser Boston)

Rizo Ph, Grangeat P and Guillemaud R 1994 Geometric calibration method for multiple-head cone-beam SPECT system *IEEE Trans. Nucl. Sci.* **41** 2748–57

Rougée A, Picard C, Ponchut C and Trousset Y 1993 Geometrical calibration of x-ray imaging chains for three-dimensional reconstruction *Comput. Med. Imaging Graphics* **17** 295–300

Tam K C 1997 Cone-beam imaging of a section of a long object with a short detector *Information Processing in Medical Imaging (Lecture Notes in Computer Science 1230)* ed J S Duncan and G R Gindi (Berlin: Springer) pp 525–30

Wang H, Smith M F, Stone C D and Jaszczak R J 1998 Astigmatic single photon emission computed tomography imaging with a displaced center of rotation *Med. Phys.* **25** 1493–501

White T A, Roney T J, Pink R J, Noo F, Clackdoyle R, Smith M and Jones W F 1999 Comparison of fan- and cone-beam imaging capabilities on a portable x-ray imaging system *Proc. SPIE* **3772** 138–46